10-15-2018

A Bismuth Attack at Grain-Boundaries of Ceria-Based Electrolytes

Tianrang Yang

Kevin Huang
University of South Carolina - Columbia, huang46@cec.sc.edu

Publication Info

Published in *Journal of The Electrochemical Society*, Volume 165, Issue 13, 2018, pages F1110-F1114.

A Bismuth Attack at Grain-Boundaries of Ceria-Based Electrolytes

Tianrang Yang * and **Kevin Huang** **,z

Department of Mechanical Engineering, University of South Carolina, Columbia, South Carolina 29208, USA

Bismuth is a common additive of commercial silver pastes for enhancing metallization effect; silver paste is also commonly used in high-temperature electrochemical cells as a current collector or contact layer. We here report that the minor amount of bismuth in commercial silver pastes can transport to the interface of electrode/Gd-doped CeO_2 (GDC) electrolyte and seriously corrode grain-boundaries (GBs) of the GDC electrolyte, a commonly used intermediate-temperature electrolyte, causing significant ionic conductivity degradation. A comprehensive electron microscopic analysis reveals that the Bi-corrosion takes place along GBs of GDC electrolyte acting as "washing flux" agent, causing grain separation and thus blocking ionic conduction. It is also found that electrical field enhances the "Bi-washing" effect, leading to a faster degradation in full-cell than in half-cell. Overall, the use of commercial silver paste as a current collector for CeO_2-based electrolytes in long-term testing should be cautioned.
 [DOI: 10.1149/2.1091813jes]

Manuscript submitted August 23, 2018; revised manuscript received September 27, 2018. Published October 15, 2018.

One of the degradation causes for electrochemical systems is the component poisoning by contaminations. For example, oxide-based air-electrodes in solid oxide fuel cells can be poisoned by chromium migrated from high-temperature metallic interconnects via a vaporization-condensation mechanism;[1–5] Ni-based fuel-electrodes can be poisoned by sulfur residue in hydrocarbon fuels via adsorption-sulfide formation mechanism;[6–7] the ionic conductivity of ZrO_2-based electrolytes can be lowered by silica even at an impurity level as low as 50 ppm.[8,9]

Ceria-based electrolytes are well-known and commonly used for intermediate-temperature solid oxide fuel cells (SOFCs), solid oxide electrolysis cells (SOECs), oxygen pumps or sensors. The impurity of silica has been reported to be detrimental to the ionic conductivity of Gd-doped CeO_2 (GDC).[10,11] Jiang, et al. has also reported that GDC was chemically incompatible with boron-containing glass sealants due to the formation of $GdBO_3$ above 600°C.[12]

In many laboratory studies, Pt or Ag paste is commonly used to provide a good contact for low-resistance current collection. However, these commercial metallization pastes contain a certain percentage of bismuth in the form of glass frit.[13–17] The impact of these Bi-containing glass frits on the performance of electrode and electrolyte with which they are in close contact has rarely been studied before. We here report that the oxide-ion conductivity of GDC electrolyte in an electrochemical cell can be seriously degraded by the bismuth present in the current collecting Ag paste. We here present strong microscopic and chemical evidence that GBs of GDC electrolytes are seriously attacked by bismuth in Ag pastes using field emission scanning electron microscopy (FESEM), transmission electron microscopy (TEM) and scanning transmission electron microscope (STEM) equipped with energy dispersive X-ray spectrometry (EDX).

Experimental

Symmetrical half-cell.—$(La_{0.6}Sr_{0.4})_{0.95}Co_{0.2}Fe_{0.8}O_{3-\delta}$ (LSCF) thin films were prepared by screen printing a commercial ink (Fuel Cell Materials, LSCF-I) on both sides of a 400-μm thick GDC20 ($Ce_{0.8}Gd_{0.2}O_{2-\delta}$, Fuelcellmaterials) membrane, followed by firing at 1100°C for 2 h. A commercial silver paste (c8829a, Heraeus) was then painted on both surfaces of LSCF as current collectors and fired at 600°C for 2 h. The surface area of LSCF or Ag paste is 1.27 cm^2. In a typical cell, the weights of LSCF and silver paste are 18.6 and 6.6 mg, respectively. The component in the paste is mainly silver with a small amount of bismuth as evidenced in Figure 1 of EDX analysis; the molar ratio of Bi/Ag from the quantification is roughly 1/30. A symmetrical half-cell was held at 700°C for 1,000 h during which electrochemical impedance spectroscopy data were collected periodically with a 1470/1455B Solartron electrochemical workstation in a frequency range of 0.1 Hz–1 MHz and AC amplitude of 10 mV.

Single cell.—A GDC10 ($Ce_{0.9}Gd_{0.1}O_{1.95}$, Fuelcellmaterials) membrane was used as the electrolyte in single cell originally because of its higher ionic conductivity than GDC20. However, we do not expect the Bi-corrosion behavior would be significantly different between the two compositions. The cell configuration was anode-supported Ni-GDC10/GDC10/LSCF. To make the anode substrate, NiO (J.T. Baker), GDC10 and carbon black (Fisher Chemical) in a weight ratio of 6:4:2 were ball-milled in ethanol for 3 h, following by drying, pelletizing with 5 wt% PVB (Polyvinyl butyral, Sigma Aldrich) binder and firing at 800°C for 2 h. To make the GDC10 electrolyte layer, a roughly 10 g GDC10 powder was first ball milled with 28.5 g ethanol solvent, 0.4 g PVB binder, 0.3 g TEA (Triethanolamine, Alfa Aesar) dispersant, 0.37 g PEG600 (polyethylene glycol-600, Alfa Aesar) and 0.37 g DBP (Dibutyl phthalate, Acros Organics) plasticizer for 24 h. Then, 200 μL of the resultant slurry (corresponding to 40 μm-thickness) was drop cast onto the surface of an anode substrate with a single-channel pipettor (100-1000 μL). The bilayer structure was then dried at room temperature for 2 h before sintering at 1500°C for 6 h. The cathodes LSCF and current collector Ag were finally applied by following the same procedures as symmetrical cells. During electrical testing, 3 vol% H_2O/97 vol% H_2 mixture at a flow rate of 100 mL/min

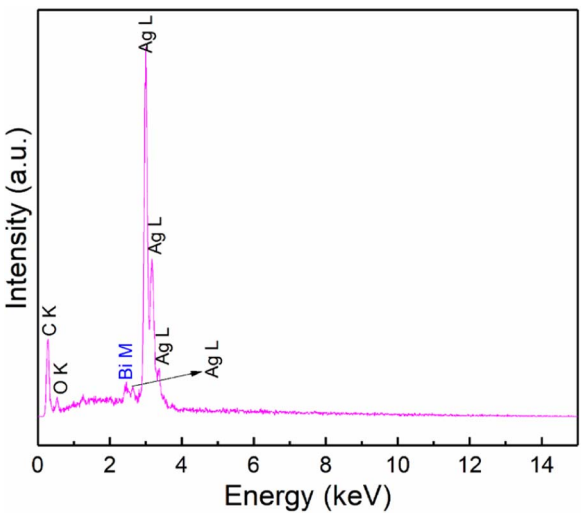

Figure 1. EDX analysis of Heraeus c8829a silver paste.

*Electrochemical Society Student Member.
**Electrochemical Society Member.
zE-mail: huang46@cec.sc.edu

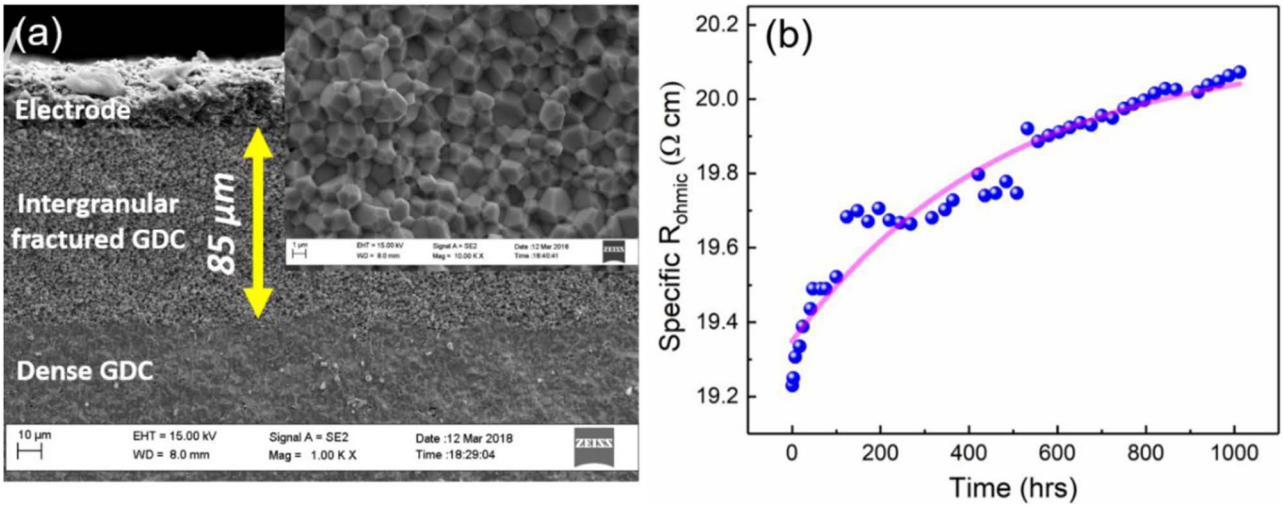

Figure 2. (a) Cross-sectional view of GDC electrolyte after testing in symmetrical half-cell at 700°C for 1,000 h; the inset is the enlarged image of intergranular fracture area; (b) time-dependent area-specific ohmic resistance of cell shown in (a).

was supplied as fuel to the anode side, while stagnant air was exposed to cathode. The cell was operated on SOFC mode at 700°C for 100 h.

Electron microscopy and EDX.—The cross-sections of post-tested samples were characterized by FESEM (Zeiss Ultra) equipped with EDX. Focused Ion Beam (FIB, Hitachi NB-5000) technique was used to prepare samples for TEM imaging (Hitachi H-9500) and selected area electron diffraction (SAED). The scanning transmission electron microscope (STEM, Hitachi HD-2000) equipped with EDX were also employed to obtain images and analyze chemical compositions. The resolutions for STEM-EDX are 0.8, 0.5 and 0.3 nm for spot, line-scan and mapping, respectively.

Results and Discussion

Morphology and ohmic resistance.—The cross-sectional view of the electrolyte in the symmetrical half-cell after EIS measurement at 700°C for 1,000 h is shown in Figure 2a. A distinct two-layer structure in the GDC electrolyte is clearly observable: a top 85 μm thick intergranular fractured layer right underneath the cathode and a bottom normal dense layer. Correspondingly, Figure 2b shows a non-linear increase in area-specific ohmic resistance, implying that performance degradation of the electrolyte is related to the fracturing of GBs in the GDC electrolyte.

The character of the above bilayer structure (fully densified + intergranular fractured layers) is also observed in the GDC electrolyte of a full fuel cell. The dense microstructure in the GDC membrane before test is clearly shown in Figure 3a. However, after operation at 700°C for just 100 hours, Figure 3b shows that the electrolyte has been seriously corroded. The grains in the GDC electrolyte near the cathode side are loosely connected or even completely detached from each other. Due to the corroded GBs in the electrolyte and subsequently deteriorated LSCF/GDC interfacial contact, the area-specific ohmic resistance is increased from 0.10 to 0.17 Ω cm^2 as seen from the EIS spectra in the inset of Figure 3b. The increased polarization resistance (R_P) of electrode is consistent with reported behavior of LSCF, likely caused by particle coarsening, Sr-segregation[18,19] and deteriorated interfacial bonding by the Bi-attack. However, we do not believe that the interaction between Bi and LSCF (to be shown later) contributes to the degradation of R_P for two reasons: 1) only very limited amount of Bi was found by EDX to enter LSCF after 1000 h test, resulting in a solid solution[20] with very low La/Bi ratio varying from 30–100/1; 2) early studies have shown that the presence of Bi in LSCF or (La, Sr)$MnO_{3-\delta}$ can in fact enhance the cathode performance.[21,22]

Microstructural and compositional analyses.—To understand what has caused the grain-boundary corrosion in the GDC electrolyte, we carried out more electron microscopic characterization. Figure 4 shows a TEM image of the post-test sample. The image was taken at 5–7 μm beneath the LSCF/GDC interface, where the intergranular fracturing is observed. Thick and clear grain boundaries are observed

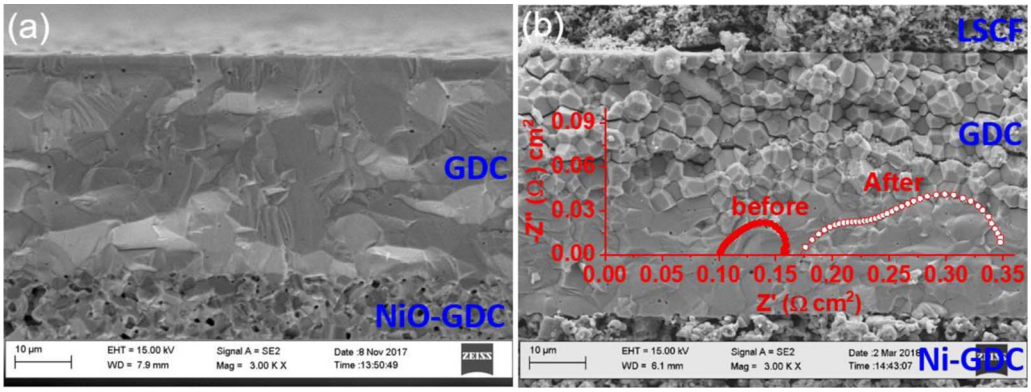

Figure 3. Cross-section images of electrolyte in a full cell. (a) before test; (b) after test. The inset in (b) show the EIS spectra before and after discharge at 700°C for 100 h.

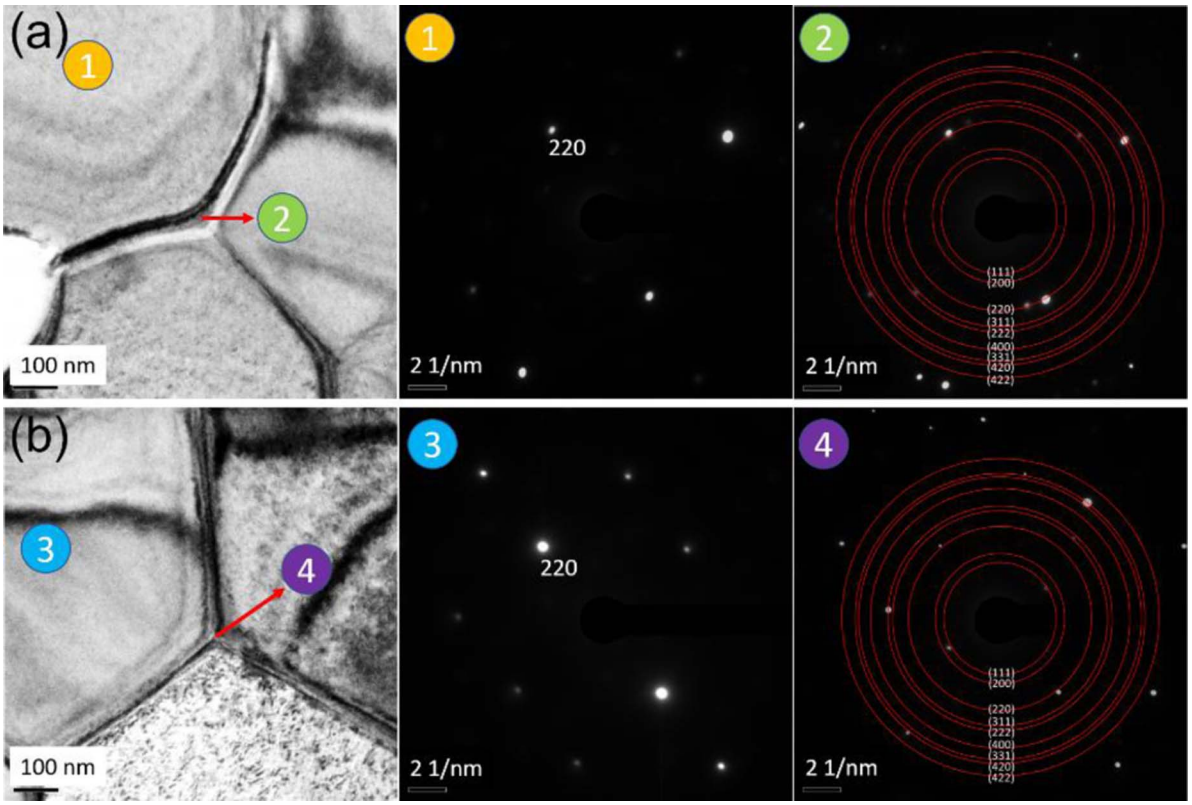

Figure 4. TEM images and SAED patterns for the electrolyte. (a) symmetrical cell after 1,000 h at 700°C; (b) fuel cell after 100 h at 700°C. The numbers mark the center of electron beam area (0.7 μm in diameter) for SAED.

for both electrolytes from symmetrical cell and full cell. The selected area electron diffraction (SAED) on grains indicate a single-crystal cubic structure related to GDC (Fm-3 m, space group# 225). The SAED on grain boundaries instead show a polycrystalline character arising from random orientations of the three neighboring grains. No secondary phase is detectable at grain boundaries since all the diffraction spots can be indexed by the same cubic structure of GDC. However, Figure 5 indicates an impurity phase between detached grains in GDC10 used in full cell. The later STEM-EDX results confirm that the impurity is a bismuth-rich material.

Figures 6a and 6b show the STEM-EDX results of grain-boundary regions in a post-tested sample for symmetrical cell and full cell, respectively. No trace of La, Sr, Fe and Ag from cathode/Ag paste migrating into the electrolyte grains can be found by STEM-EDX. The amounts of Co are also negligible. Notably, only Bi is present at grain boundaries for both samples, suggesting that it might be the culprit of the observed intergranular fracturing along GBs. The elemental analysis for the embedded "chips" shown in Figure 6c between two grains of GDC10 used in the full cell testing also indicates a bismuth-dominated composition with minor La, Sr, Ce and Gd. From the EDX results, the apparent composition of the "chips" can be expressed by $Bi_{1.48}Sr_{0.20}La_{0.17}Gd_{0.08}Ce_{0.07}O_{3-\delta}$ with a very small amount of Fe neglected. This phenomenon is similar to what was reported by Cao et al.,[23] where polycrystalline YSZ or GDC was

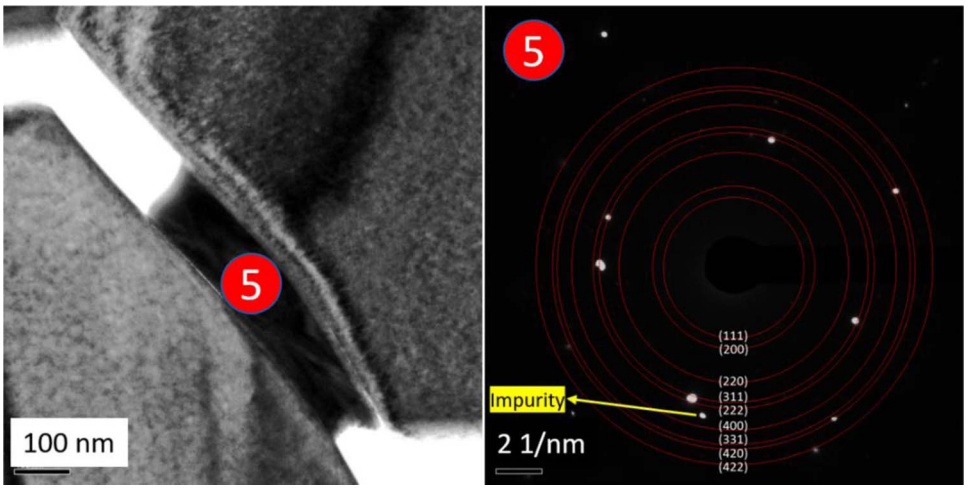

Figure 5. TEM image and SAED pattern for electrolyte in a post-tested full cell at a position 5–7 μm beneath the cathode/electrolyte interface.

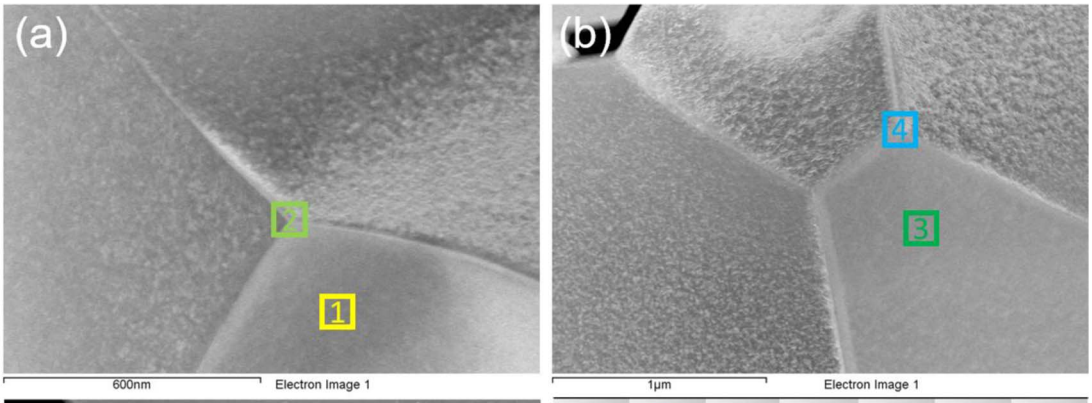

	1	2	3	4	5	6
Ce	1	1	1	1	1	1
Gd	0.228	0.179	0.124	0.087	0.123	1.095
La	0	0	0	0	0	2.536
Sr	0	0	0	0	0	2.917
Co	0.010	0	0	0.007	0.007	0
Fe	0	0	0	0	0	0.333
Ag	0	0	0	0	0	0
Bi	0	0.059	0	0.030	0	21.500

Figure 6. STEM-EDX images and quantification results for GDC electrolyte in post-tested cells at a position 5–7 µm beneath the cathode/electrolyte interface. (a) Symmetrical cell; (b) full cell; (c) a focused grain boundary region from an electrolyte used in full cell testing. The table lists the compositions (molar ratio normalized to Ce amount) for each area shown in (a), (b) and (c).

corroded by liquid Sb_2O_3, but not in single crystal YSZ due to the lack of grain boundaries. The corrosion of GDC observed in this work likely follows a similar mechanism that Bi migrates along grain boundaries and weakens the bonding between grains.

Furthermore, the oxygen-ion current flow present in full cell testing is also found to accelerate the electrolyte grain-boundary corrosion; this is clearly seen from the degree of damage in the 100-h full cell testing vs 1,000-h symmetrical cell testing at 700°C, compare Figures 2 and 3. The faster attacking rate in full cell probably arises from the faster migration of ions along the grain-boundary under an electrical field.[24–26] Since Bi_2O_3 itself is an excellent oxide-ion conductor, we expect electrical field would push oxide-ion with Bi-ion (required by charge neutrality) through GBs, thus resulting in an accelerated mass transport.

A proposed corrosion mechanism.—Based on the above spectral analysis at GBs of GDC, we here propose a Bi-corrosion mechanism as follows. The Bi_2O_3 in Ag paste first reacts with LSCF, forming a Bi-rich eutectic compound; the latter then migrates toward the LSCF/GDC interface, where the eutectic flux attacks GBs of GDC, resulting in a composition as revealed by STEM/EDX analysis in Figure 6. The proposed mechanism is supported by both our observation and literature. Figure 7 shows a direct observation of liquid-phase residue on the surfaces of LSCF particles as well as GBs of the GDC electrolyte after testing. The formation of a eutectic liquid phase between Bi and LSCF has also been directly observed by Fan et al. when only 1% Bi_2O_3 (mol%) was added into LSCF ($La_{0.54}Sr_{0.44}Co_{0.2}Fe_{0.8}O_{3-\delta}$) at 800°C.[21] From other studies, the tendency of Bi_2O_3 to form eutectic compounds $Bi_{2-x}M_xO_{3-\delta}$ (M = La and Sr) with SrO[27,28] and La_2O_3[29]

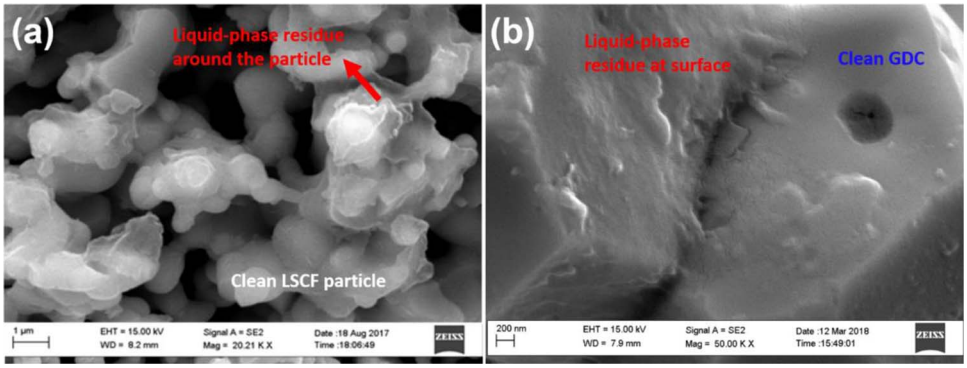

Figure 7. SEM images of (a) LSCF and (b) GDC in a post-tested full cell.

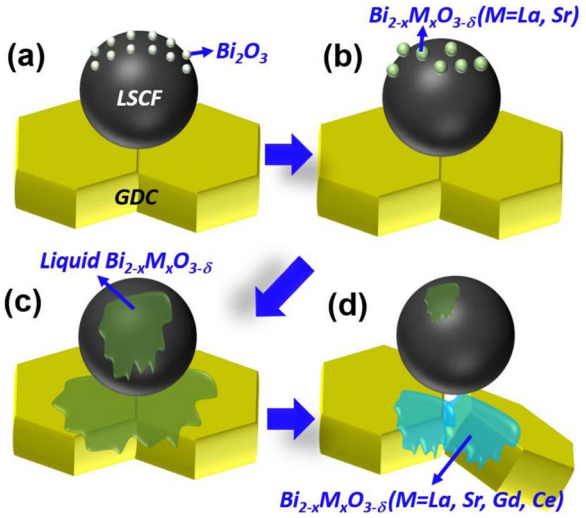

Figure 8. A schematic illustrating the mechanism of Bi-corrosion at GBs of GDC electrolytes.

has also been confirmed. When in contact with GDC, Ce and Gd can also be dissolved to form $Bi_{2-x}M_xO_{3-\delta}$ (M = La, Sr, Gd and Ce).[29] To facilitate the understanding of the proposed Bi-corrosion mechanism, we schematically illustrate the overall process in Figure 8.

A rough estimate of the thickness of the formed Bi-rich liquid phase as a film as it migrates can be estimated as follows. The weights of Ag paste and LSCF-cathode used in this study are 6.6 and 18.6 mg, respectively, whereas the molar ratio of Bi/Ag in the Ag paste determined by EDX is ~1/30 (averaged from two samples, ranging from 1.93/60.92 to 1.50/42.65). Combined these values with the known cell geometry and material density, the calculated weight ratio of Bi_2O_3/LSCF is 1/42 and the thickness of the film is roughly 0.2 μm if it is uniformly distributed on the GDC surface.

Conclusions

In summary, an ionic conductivity degradation in the GDC electrolyte was observed after testing in either half-cell or full-cell configuration. Subsequent electron microscopic studies revealed that the degradation is associated with drastic microstructural change along GBs in the GDC electrolyte layer, i.e. intergranular separation of grains. A further chemical analysis at GBs indicates the presence of Bi. The origin of Bi was found to be from the commercial silver paste used for current collection, in which Bi is commonly used as a flux material to enhance the metallization. Therefore, the GBs corrosion phenomenon can be understood by Bi_2O_3 first reacting with cathode LSCF, forming a eutectic liquid that continues to flow and "washing" through GBs of the GDC electrolyte, weakening the grain-grain bonding and thus causing conductivity decay. It is also found that electrical field enhances the "Bi_2O_3-washing" phenomenon, thus resulting in a faster degradation of GDC conductivity in full-cell than in half-cell.

Acknowledgment

We thank National Energy Technology Laboratory (NETL) of Department of Energy for supporting this work through an award DE-FE-0031176.

ORCID

Tianrang Yang https://orcid.org/0000-0003-0843-4236
Kevin Huang https://orcid.org/0000-0002-1232-4593

References

1. J. A. Schuler, Z. Wuillemin, A. Hessler-Wyser, C. Comminges, and N. Y. Steiner, *J. Power Sources*, **211**, 177 (2012).
2. H. Yokokawa, T. Horita, N. Sakai, K. Yamaji, M. Brito, Y.-P. Xiong, and H. Kishimoto, *Solid State Ion.*, **177**, 3193 (2006).
3. E. Park, S. Taniguchi, T. Daio, J.-T. Chou, and K. Sasaki, *Solid State Ion.*, **262**, 421 (2014).
4. E. Park, S. Taniguchi, J.-T. Chou, Y. Tachikawa, Y. Shiratori, and K. Sasaki, *ECS Trans.*, **50**, 21 (2013).
5. S. Taniguchi, M. Kadowaki, H. Kawamura, T. Yasuo, Y. Akiyama, Y. Miyake, and T. Saitoh, *J. power sources*, **55**, 73 (1995).
6. A. Hauch, A. Hagen, J. Hjelm, and T. Ramos, *J. Electrochem. Soc.*, **161**, F734 (2014).
7. M. Riegraf, G. Schiller, R. Costa, K. A. Friedrich, A. Latz, and V. Yurkiv, *J. Electrochem. Soc.*, **162**, F65 (2015).
8. T. Carvalho, E. Antunes, J. Calado, F. M. Figueiredo, and J. R. Frade, *Solid State Ion.*, **225**, 484 (2012).
9. Y. Liu, *Solid State Ion.*, **161**, 1 (2003).
10. J.-M. Bae and B. Steele, *Solid State Ion.*, **106**, 247 (1998).
11. S.-Y. Park, P.-S. Cho, S. B. Lee, H.-M. Park, and J.-H. Lee, *J. Electrochem. Soc.*, **156**, B891 (2009).
12. K. Chen, N. Ai, and S. P. Jiang, *Fuel Cells*, **13**, 1101 (2013).
13. A. Hashimoto, T. Yasuho, M. Hayama, K. Miura, and Conductive paste, *Google Patents* (2002).
14. S. Shahbazi, S. Grabey, and M. Challingsworth, Platinum containing conductive paste, *Google Patents* (2018).
15. L. Wang, L. Yan, C. Guo, and W. Zhang, Inorganic reaction system for electroconductive paste composition, *Google Patents* (2016).
16. R. Prunchak and Glass frits, *Google Patents* (2010).
17. A. Bechtloff, A. Niemann, and S. Schreiber, Conductive paste, article produced therewith with a conductive coating on glass, ceramic or enameled steel and method for the production thereof, *Google Patents* (2004).
18. D. Oh, D. Gostovic, and E. D. Wachsman, *J. Mater. Res.*, **27**, 1992 (2012).
19. H. Wang, K. J. Yakal-Kremski, T. Yeh, G. M. Rupp, A. Limbeck, J. Fleig, and S. A. Barnett, *J. Electrochem. Soc.*, **163**, F581 (2016).
20. V. Kharton, E. Naumovich, and V. Samokhval, *Solid State Ion.*, **99**, 269 (1997).
21. B. Fan, J. Yan, and W. Shi, *J. Eur. Ceram. Soc.*, **30**, 1803 (2010).
22. N. Ai, J.-P. Veder, Y. Cheng, M. Chen, K. Chen, T. Zhang, and S. P. Jiang, *J. Electrochem. Soc.*, **164**, F1471 (2017).
23. T. Cao, Y. Cheng, R. J. Gorte, Y. Shi, J. M. Vohs, and N. Cai, *Ceram. Int.*, **43**, 16575 (2017).
24. R. Rosenberg and M. Ohring, *J. Appl. Phys.*, **42**, 5671 (1971).
25. I. A. Blech, *J. Appl. Phys.*, **47**, 1203 (1976).
26. C. Gan and M. Lim, in *Electromigration in Thin Films and Electronic Devices*, p. 113, Elsevier (2011).
27. D. Risold, B. Hallstedt, L. Gauckler, H. Lukas, and S. Fries, *J. phase equilibria*, **16**, 223 (1995).
28. R. Guillermo, P. Conflant, J. Boivin, and D. Thomas, *Rev. Chim. Miner.*, **15**, 153 (1978).
29. E. M. Levin and R. S. Roth, *J. Res. Natl. Bur. Stand. A*, **68**, 197 (1964).